AIP | Review of Scientific Instruments

Development of a balanced detector with biased synchronous detection and application to near shot noise limited noise cancelling of supercontinuum pulse light

Keisuke Seto, Toshiaki Tsukada, Yoshinao Okuda, Eiji Tokunaga, and Takayoshi Kobayashi

Citation: Review of Scientific Instruments **85**, 023702 (2014); doi: 10.1063/1.4863879
View online: http://dx.doi.org/10.1063/1.4863879
View Table of Contents: http://scitation.aip.org/content/aip/journal/rsi/85/2?ver=pdfcov
Published by the AIP Publishing

Development of a balanced detector with biased synchronous detection and application to near shot noise limited noise cancelling of supercontinuum pulse light

Keisuke Seto,[1,2] Toshiaki Tsukada,[3] Yoshinao Okuda,[4] Eiji Tokunaga,[4] and Takayoshi Kobayashi[1,2,5,6]

[1]*Advanced Ultrafast Laser Research Center, The University of Electro-Communications, 1-5-1, Chofugaoka, Chofu, Tokyo 182-8585, Japan*
[2]*CREST, Japan Science and Technology Agency, 4-1-8, Honcho, Kawaguchi, Saitama 332-0012, Japan*
[3]*Keisoku Solution Co., Ltd., Haitsu enomoto B1F, 3-32-18, Nukuikitamachi, Koganei-shi, Tokyo 184-0015, Japan*
[4]*Department of Physics, Faculty of Science, Tokyo University of Science, 1-3 Kagurazaka, Shinjuku-ku, Tokyo 162-8601, Japan*
[5]*Department of Electrophysics, National Chiao-Tung University, Hsinchu 300, Taiwan*
[6]*Institute of Laser Engineering, Osaka University, 2-6 Yamada-oka, Suita, Osaka 565-0971, Japan*

(Received 13 September 2013; accepted 16 January 2014; published online 5 February 2014)

We report on the development of a balanced detector suited for multicolor imaging. The source pulsed light is split into probe and reference pulsed light. The reference pulse is delayed through an optical path and the probe and reference pulses are detected by a single photodetector. The signs of the detected signals of the probe and reference pulses are flipped based on a signal synchronous to the light source. Then, the signals are averaged through a low-pass filter. The output signal is proportional to the intensity difference between the probe and the reference. This balanced detector has two features: (1) both the probe and reference pulsed lights are detected by a single photodetector and (2) a voltage bias on the sign flipping compensates for the optical-intensity unbalance between the probe and reference pulsed lights. The first feature enables the probe and reference pulses to travel along a common optical path from a sample through a spectrograph to the photodetector, which minimizes the intensity unbalance between the probe and reference pulses during imaging and spectroscopy. The second feature ensures the complete balanced-detection in whole wavelength range by compensating for the optical unbalance created by deviations in the splitting ratios of the probe and reference lights at different wavelengths. Although a higher signal to noise ratio (SNR) reached to near shot noise limited SNR is attained by attaching a resonator to the photodetector for pulse repetition, the electrical bias cannot compensate for the optical balance. This unbalance is, however, corrected by adjusting the phase of the synchronous signal. We applied the present balanced detection to a stimulated Raman microscope with supercontinuum probe light and demonstrated its noise cancelling performance through capturing polystyrene beads. © *2014 AIP Publishing LLC*. [http://dx.doi.org/10.1063/1.4863879]

I. INTRODUCTION

A single-shot multi-color imaging method is demanded in various fields. Such imaging is attained with a white-light source. A broadband femtosecond pulse from a titanium-sapphire oscillator can be used as the white light, and has been applied to multiplex coherent anti-stokes Raman scattering (CARS)[1] and stimulated Raman scattering (SRS) microscopies.[2,3] This light source is stable and even the shot-noise limited signal to noise ratio (SNR) can be attained.[3] However, in the pump-probe measurements with this type of probe-light source, an additional pump-light source is often necessary,[2,3] which significantly increases the cost and requires the synchronization of these light sources within the pulse durations.

A supercontinuum (SC) light source with a photonic crystal fiber (PCF)[4] is a promising candidate for such imaging due to octave-spanning-wavelength white light generation with low input pulse-energy, and has been applied in fluorescent microscopy,[5–7] CARS microscopy,[8,9] SRS microscopy,[10–12] and so on.[13] Although the generation of the SC light by the PCF provides low-cost systems, easy handling, and adjustment of the optics, rendering the additional pump light source and an optical amplifier unnecessary, the SC pulsed light is significantly unstable and can result in very high levels of source-induced noise,[14–18] which is a serious obstacle to high-speed multi-color imaging applications. To overcome this problem, the nature of the noise has been studied[14–18] and several noise reduction methods[19–21] have been developed.

Another way to solve this problem is through the development of noise cancelling methods, one of which is balanced detection.[22,23] The source light is split into probe and reference lights. Only the probe light is used to measure a sample, then both lights are detected by the other detectors and the detected signal of the reference light is subtracted from that of the probe light. The optical intensity noises appear in-phase on the probe light and the reference signals, and measured information only appears on the probe light. Thus, only the noise is cancelled out by the subtraction. However,

this balanced detection has the following problems. First, the probe and reference lights are detected through different optical paths, which create an artifact image through undesirable effects such as reflection, scattering, and/or absorption by the sample, which modulate only the probe light. It is desirable for the light paths of both the probe and reference lights to go through the same sample position to also subtract these effects. Second, the probe and reference lights are detected by different detectors, which is problematic, particularly when applied to spectroscopy with the SC light. In the balanced detection for each wavelength through dispersing the white light, the probe and reference lights must be dispersed and detected in exactly the same conditions, due to the spectrally uncorrelated nature of the noise.[24] The detection of the probe and reference lights by the different detectors requires the rigorous operation of two spectrographs in the same state, which significantly complicates the system. Therefore, it is desirable in spectroscopy for both lights to be detected by a single photodetector through a single spectrograph. Furthermore, even for various applications such as sensors and imaging systems using comparative type schemes, the desired goal is detection without unbalance.

The first problem of the intensity unbalance between the probe and reference lights can be solved with the auto-balanced scheme.[25] In this scheme, the probe and reference lights are detected by different photodetectors, and the gains of the pre-amplifiers for each lights are dynamically controlled to correct the intensity unbalance based on their direct current (DC) components of the outputs. The response speed of the dynamic gain control is set as sufficiently faster than the speed of scanning in the imaging and adequately slower than the speed of the intensity modulation (signal) of the probe light. However, the auto-balanced scheme still cannot solve the abovementioned second problem in spectroscopy attributed to the different detectors for the probe and reference lights.

The abovementioned problems can be solved by the collinear balanced detection (CBD) method,[26] in which both the probe and reference lights are lock-in detected by a single PD. The arrival of the reference light is optically delayed against that of the probe light for half of the lock-in cycle. However, this method is not suited for simultaneous multi-color imaging with white light. The degree of the noise cancelling directly depends on the balance between the optical intensities of the probe and reference lights. Therefore, the equal intensities of the probe and reference lights are required at any wavelength, simultaneously. Unfortunately, the equal splitting of the white light at whole wavelengths is difficult for practically applicable optics. Some detection devices and/or methods are needed to compensate for this optical unbalance.

In this paper, we report the development of a balanced detector that solves the abovementioned problems, and show that it is suited for the multi-color imaging with the white light. In this method, the probe and reference lights are detected by a single detector, which allows for the elimination of artifact signals other than the stimulation on the sample and enables the spectral dispersion of the probe and reference lights through a single spectrograph. Furthermore, the optical unbalance between the probe and reference lights' intensities is compensated electrically in the circuit. In our method, the optical paths of the probe and reference lights are common through the sample, and thus the auto-balanced scheme is not necessary due to common effects by the sample other than stimulation by the pump light. Through these features, the developed balanced detector provides complete noise cancelling, simultaneously, at any wavelength.

Additionally, the effect of this balanced detection is demonstrated through its application to the SRS microscopy of polystyrene (PS) beads with the monochromatic pump light and white probe light of the SC light from the PCF.[11] In observation of the SRS signals, at least two pulsed lasers at different wavelengths are precisely overlapped spatially and temporally on the sample. When the energy difference between the pump and probe lights equates to a vibrational energy of a molecule, a photon of the higher energy light is annihilated and a photon of the lower energy light is generated. The SRS signals are observed as a reduction in the intensity of the shorter wavelength or an increase in that of the longer wavelength. These reduction and increase are due to stimulated Raman loss and gain process, respectively. In this paper, the stimulated Raman loss signal of the PS beads is observed and images of the beads are captured with the white probe-light of shorter wavelength and the monochromatic pump-light of longer wavelength.

II. PRINCIPAL OF OPERATION

Figure 1 is a block diagram of the balance detection system. White pulsed light is split into probe and reference pulsed lights. The reference pulse is delayed by about half the cycle of the repetition through the additional optical path. The probe and reference pulses are spatially overlapped on a beam splitter, aligned collinearly, and irradiated on a sample with the pump pulse synchronous only to the probe pulse. Then, the probe and reference pulses are spectrally dispersed by the common spectrograph and a wavelength component is input to a common fast PD. The detected signals are amplified to an appropriate level by a pre-amplifier (PA) and sent to a multiplier (ML).

The synchronous signal is sent to a band pass filter (BPF) of pulse-repetition frequency to obtain the fundamental

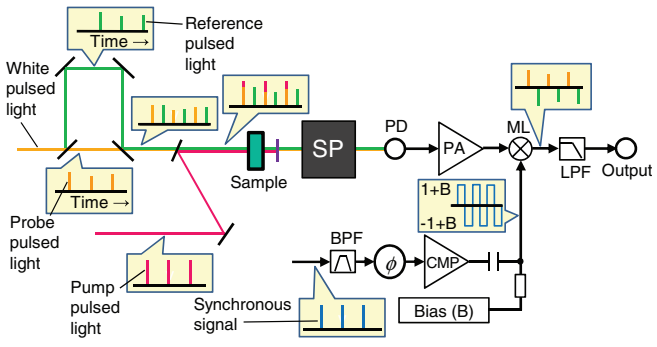

FIG. 1. Block diagram of the developed balanced-detection system. SP: spectrograph; PD: photodetector; PA: pre-amplifier; ML: multiplier; BPF: band-pass filter; ϕ: phase shifter; CMP: comparator; B: bias for compensation of the unbalance between the probe signal and the reference signal; LPF: low-pass filter.

sinusoidal signal, and its phase is adjusted by a phase shifter (ϕ). The sinusoidal signal is converted to a square wave by the comparator (CMP). A voltage bias (B) is applied to the square wave to compensate for the unbalance between the probe and reference pulses, and then sent to the ML. The signs of the probe and reference pulses are flipped in the ML by the square wave. The output from the ML is averaged through a low-pass filter (LPF), and thus the output is $(1 + B) \times$ (probe signal) $+ (-1 + B) \times$ (reference signal) or $(1 + B) \times$ (reference signal) $+ (-1 + B) \times$ (probe signal). The output is the difference signal between the probe and reference signals.

The common optical path from the sample through the spectrograph to the detector enables common spectral dispersion with the single spectrograph of the white probe and reference pulses, completing noise cancellation for each wavelength. The square wave for sign flipping renders the strict half-cycle delay of the pulse repetition unnecessary for the reference pulse, which simplifies the adjustment of the optical path. The sharp flank of the square wave also enables the application of a low repetition-rate pulsed-laser system. It is essential to compensate for the optical unbalance by using the balanced detector when applying to spectroscopy. The ratios of splitting the white pulse light into the probe and reference pulses vary in different wavelengths due to imperfections in optical devices, such as beam splitters. The optical unbalance results in imperfect noise cancelling at some wavelengths. This problem is solved by using the circuit to compensate for the deviation of the splitting ratio, and complete noise cancellation is realized in the whole wavelength region simultaneously by preparing the balanced detector for each wavelength.

The signal intensity, compared to the circuit noise (CN), can be enhanced by a resonator of its resonant frequency at the pulse repetition attached to the input of the PA. This circuit noise is due to the thermal noise of resistors, active devises such as operation amplifiers (OP amp.) and ML, dark current shot noise of the PD, and exogenous noise, which are independent of light input power. However, the signals are detected as alternative current (AC) in this case, and thus the B does not compensate for the optical unbalance. Additionally, the noise cancelling performance is more sensitive to the optical delay of the reference pulse. The optical unbalance can, however, be addressed by adjusting the optical delay and the phase of the synchronous signal as described in the following.

Let the resonated probe and reference signals and the biased square wave be expressed in the time domain as p(t), r(t), and sq(t), respectively:

$$\mathrm{p}(t) = a\,(1 + \mathrm{s}(t) + \mathrm{n}(t)) \exp\left(j\frac{2\pi}{T}t\right) + \mathrm{c.c.}, \tag{1}$$

$$\mathrm{r}(t) = b\,(1 + \mathrm{n}(t - \Delta T)) \exp\left(j\frac{2\pi}{T}(t - \Delta T)\right) + \mathrm{c.c.}, \tag{2}$$

$$\begin{aligned}\mathrm{sq}(t) &= \sum_{k=-\infty}^{\infty} 2\mathrm{rect}\left(\frac{t - kT - \delta}{T/2}\right) - 1 + B \\ &= \sum_{k=-\infty}^{\infty} \frac{2}{\pi k} \sin\left(\frac{\pi k}{2}\right) \exp\left\{j\frac{2\pi}{T}k(t - \delta)\right\} - 1 + B,\end{aligned} \tag{3}$$

where j, c.c., T, ΔT, s(t), and n(t) are the imaginary unit, the complex conjugate, the repetition period, the optical delay of the reference pulse, the optical signal intensity to be observed, and the optical intensity noise, respectively. The symbols a and b are the optical splitting weights ($a + b = 1$). The δ determines the delay of the square wave against the probe signal, and $\delta = 0$ indicates that the peaks of the probe signal are positioned at the centers of the square-wave boxes. The output signal from the ML is calculated as follows:

$$\begin{aligned}&(\mathrm{p}(t) + \mathrm{r}(t))\,\mathrm{sq}(t) \\ &= \frac{4}{\pi} a\,\mathrm{s}(t) \cos\left(\frac{2\pi}{T}\delta\right) + \frac{4}{\pi}\left[a\,(1 + \mathrm{n}(t)) \cos\left(\frac{2\pi}{T}\delta\right)\right. \\ &\quad \left. + b\,(1 + \mathrm{n}(t - \Delta T)) \cos\left\{\frac{2\pi}{T}(\delta - \Delta T)\right\}\right] \\ &\quad + (\text{high-frequency components}).\end{aligned} \tag{4}$$

This output is averaged through the LPF. The output from the LPF of time constant (TC) of τ ($\gg T$) is as follows:

$$\begin{aligned}&\int_{-\infty}^{t} (\mathrm{p}(s) + \mathrm{r}(s))\mathrm{sq}(s) \exp\left(-\frac{t - s}{\tau}\right) ds \\ &\cong \frac{4}{\pi} a\,\cos\left(\frac{2\pi}{T}\delta\right) \langle \mathrm{s}(t)\rangle_\tau + \frac{4}{\pi} a\,\cos\left(\frac{2\pi}{T}\delta\right)(\tau + \langle \mathrm{n}(t)\rangle_\tau) \\ &\quad + \frac{4}{\pi} b\,\cos\left\{\frac{2\pi}{T}(\delta - \Delta T)\right\} \exp\left(\frac{\Delta T}{\tau}\right) \\ &\quad \times \left[\tau + \langle \mathrm{n}(t)\rangle_\tau - \int_{t-\Delta T}^{t} (1 + \mathrm{n}(s)) \exp\left(-\frac{t - s}{\tau}\right) ds\right],\end{aligned} \tag{5}$$

where

$$\langle f(t)\rangle_\tau := \int_{-\infty}^{t} \mathrm{f}(s) \exp\left(-\frac{t - s}{\tau}\right) ds. \tag{6}$$

When the time constant of the LPF is sufficiently lager than the optical delay ($\tau \gg \Delta T$), the terms are approximated as follows:

$$\exp\left(\frac{\Delta T}{\tau}\right) \cong 1, \tag{7}$$

$$\tau + \langle \mathrm{n}(t)\rangle_\tau \gg \int_{t-\Delta T}^{t} (1 + \mathrm{n}(s)) \exp\left(-\frac{t - s}{\tau}\right) ds. \tag{8}$$

The output signal is thus expressed as follows:

$$\begin{aligned}\text{output} \propto\ & a\,\cos\left(\frac{2\pi}{T}\delta\right) \langle \mathrm{s}(t)\rangle_\tau + \tau\left[a\,\cos\left(\frac{2\pi}{T}\delta\right) + b\,\cos\left\{\frac{2\pi}{T}(\Delta T - \delta)\right\}\right] \\ &+ \sqrt{\left[\left[a\,\cos\left(\frac{2\pi}{T}\delta\right) + b\,\cos\left\{\frac{2\pi}{T}(\Delta T - \delta)\right\}\right] \langle \mathrm{n}(t)\rangle_\tau\right]^2 + 2\mathrm{CN}^2 + 2\mathrm{SN}^2}.\end{aligned} \tag{9}$$

The value of B is found to have no effect on the output, as expressed in Eq. (9), and the B term cannot compensate for the optical unbalance (a ≠ b). Here, the SN is derived from shot noise of optical current of the PD. The SN is proportional to the square root of the optical current. The SN is also proportional to the absolute value of the gain of the circuit for optical input determined by δ and ΔT. Note that the noise powers are doubled due to two time measurements of the optical currents for the probe and reference lights.

When the optical delay is set as the half cycle of the repetition ($\Delta T = T/2$), the output and SNR are calculated as follows:

$$\text{output} \propto a\ \cos\left(\frac{2\pi}{T}\delta\right)\langle \text{s}(t)\rangle_\tau + \tau\,(a-b)\cos\left(\frac{2\pi}{T}\delta\right) + \sqrt{\left\{(a-b)\ \cos\left(\frac{2\pi}{T}\delta\right)\langle \text{n}(t)\rangle_\tau\right\}^2 + 2\text{CN}^2 + 2\text{SN}^2}, \tag{10}$$

$$\text{SNR} = \frac{\left|a\ \cos\left(\frac{2\pi}{T}\delta\right)\langle \text{s}(t)\rangle_\tau\right|}{\sqrt{\left\{(a-b)\ \cos\left(\frac{2\pi}{T}\delta\right)\langle \text{n}(t)\rangle_\tau\right\}^2 + 2\text{CN}^2 + 2\text{SN}^2}}. \tag{11}$$

The SNR is maximized when the probe and reference signals are optically balanced ($a = b$) and the term δ is set to 0. The optical unbalance (the case of $a \neq b$) cannot be addressed by adjusting any parameters, and this unbalance limits the SNR. The selection of ΔT as an appropriate value, however, enables the compensation for this unbalance. By setting ΔT to, for example, the quarter cycle ($\Delta T = T/4$), the output and the SNR are represented as follows:

$$\text{output} \propto a\ \cos\left(\frac{2\pi}{T}\delta\right)\langle \text{s}(t)\rangle_\tau + \tau\sqrt{a^2+b^2}\sin\left(\frac{2\pi}{T}\delta+\alpha\right) + \sqrt{\left\{\sqrt{a^2+b^2}\sin\left(\frac{2\pi}{T}\delta+\alpha\right)\langle \text{n}(t)\rangle_\tau\right\}^2 + 2\text{CN}^2 + 2\text{SN}^2};\quad \alpha = \tan^{-1}\frac{a}{b}, \tag{12}$$

$$\text{SNR} = \frac{\left|a\ \cos\left(\frac{2\pi}{T}\delta\right)\langle \text{s}(t)\rangle_\tau\right|}{\sqrt{\left\{\sqrt{a^2+b^2}\sin\left(\frac{2\pi}{T}\delta+\alpha\right)\langle \text{n}(t)\rangle_\tau\right\}^2 + 2\text{CN}^2 + 2\text{SN}^2}}. \tag{13}$$

Here, the residual optical noise caused by the unbalance is canceled out by adjusting the δ term as follows:

$$\frac{2\pi}{T}\delta + \alpha = z\pi, \tag{14}$$

where z is an integer value. In this case, the SNR is maximized when the intensities of the probe and reference signals are balanced ($a = b$), and $\delta = T/4 + z\pi$. When the CN is the dominant noise source, the maximum SNR is reduced by a factor of $1/\sqrt{2}$, compared to that in the case of $\Delta T = T/2$, due to $1/\sqrt{2}$ reduction of the circuit gain for the signal and independence of the CN on this gain. However, when the SN is dominant, the maximum SNR is the same as the case of $\Delta T = T/2$, since the SN is also factored by $1/\sqrt{2}$ reduction of the gain for optical input.

III. ELECTRICAL CIRCUIT OF BALANCED DETECTOR

The circuits around the PD and the PAs are shown in Fig. 2. Details of the residual circuits are shown in the supplementary material.[24] An avalanche photo-diode (APD) (S5343, HAMAMATSU) reverse biased at 150 V is used as the fast PD. The PAs are based on OP amp. of LMH6609 and prepared in two forms.

The first form (Fig. 2(a)) is composed of a 510 Ω transimpedance amplifier (TIA) for direct signal amplification. No compensation capacitor is inserted in the feedback loop of the TIA. The bandwidth of the TIA is given by the geometric mean value of the corner frequency of the feedback loop and the unity-gain bandwidth of the OP amp. At this mean frequency, the feedback effect disappears. From 15 pF junction capacitance of the APD and the 510 Ω feedback register, the corner frequency is calculated as 20 MHz. The unity-gain bandwidth of the LMH6609 is 900 MHz, and thus the bandwidth of the TIA is 136 MHz. This TIA is followed by a 24.6 dB amplifier of 3 cascaded 8.2 dB inverting amplifiers. Although the designed gains of the respective amplifiers are 13.5 dB, the actual measured values are 8.2 dB.

The second (Fig. 2(b)) is a 6 dB non-inverting amplifier with a resonator (resonant amplifier, RA) followed by the 24.6 dB amplifier mentioned above. The resonant load-impedance of the resonator is 750 Ω. The input impedance of the OP amp. is sufficiently large and thus the non-inverting amplifier functions as a buffer for the resonator. The resonator

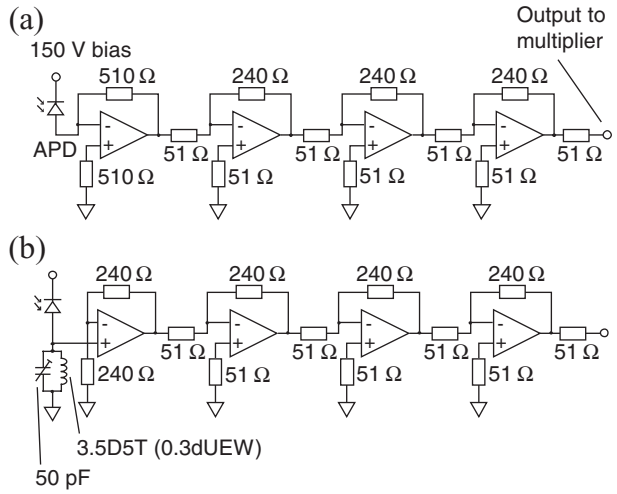

FIG. 2. Circuit diagrams of the pre-amplifiers. (a) Transimpedance amplifier for direct signal amplification. APD: avalanche photo-diode. (b) Resonant amplifier. The resonant frequency equates to the pulse repetition.

enhances the gain of the amplifier only around resonant frequency and higher SNR is expected. Note that the resonance frequency is determined not only by the capacitance and the inductance of the elements but also by the junction capacitance of the APD, the floating capacitance, and the floating inductance.

The multiplier is AD835. The value of δ is adjusted by the cable length and/or by a feedback capacitance of an OP amplifier based phase shifter. The LPF for the averaging of the sign-flipped signals is composed of 16 kHz cut-off RC passive-LPF. The signal is then filtered through a 9 kHz cut-off active-LPF and a 0.4 kHz cut-on active high-pass filter with 20 dB gain to increase the dynamic range.

IV. OPTICAL SETUP

The experimental setup (Fig. 3) is slightly modified from that in our previous work.[11] The light source is a mode-locked titanium-sapphire oscillator (Mira 900P, COHERENT). The duration time, repetition rate, and average power are 2.5 ps, 76.3 MHz, and 550 mW, respectively. The back-reflected light from the optics is rejected by a Faraday isolator (I-7090C-2H, ISOWAVE) to protect the laser from instability. The pulsed laser beam is split into two by a beam splitter (BS1) with 67% transmissivity (T) and 33% reflectivity (R), corresponding to the probe and pump lines, respectively.

The 67% transmitted beam is introduced into a microscope objective (40× magnification, numerical aperture (NA) = 0.65) and coupled with a 18.8-cm-long piece of PCF. The PCF (PM-NL-750, NKT) is of the polarization-maintaining type. The angle of the polarization plane of the input light is adjusted by a half-wave plate to maximize the efficiency of the conversion into white light. The output light is collimated by another microscope objective lens (40×, NA = 0.65). The polarization plane of the collimated white light is adjusted with a Glan-Thompson prism (GTPC-08-20AN, SIGMAKOKI). The beam diameter is expanded by a 1.5 × inverted Galilean telescope with a $f = -100$-mm concave lens and a $f = 150$-

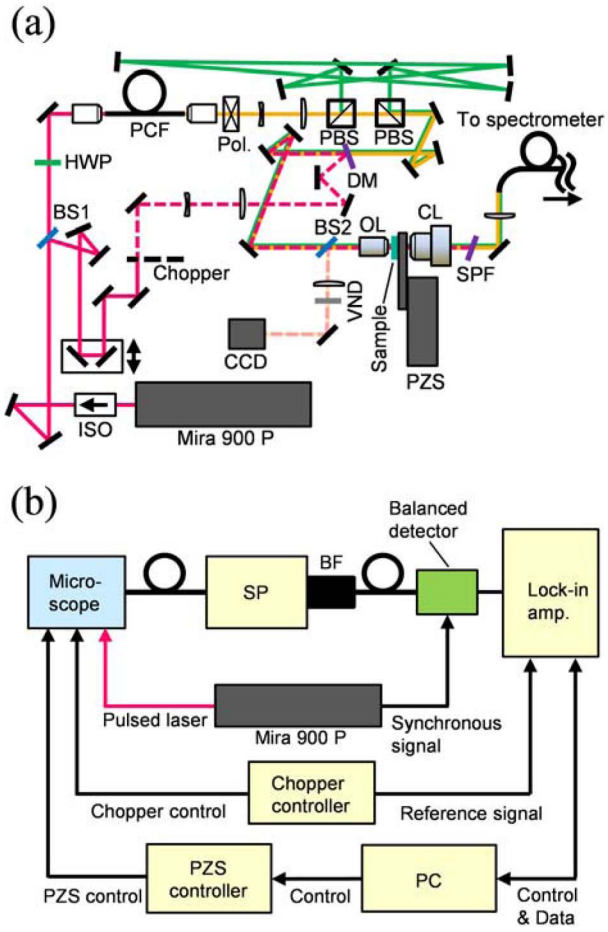

FIG. 3. Optics for stimulated Raman microscope equipped with the developed balanced detector (a) and electronic connections among the balanced detector, the light source, the controllers, and the lock-in amplifier (b). (a) The red, orange, and green lines show the pump light at 800 nm, the white probe light, and the white reference light, respectively. ISO: isolator; BS1: beam splitter for the pump light and the white light line; HWP: half-wave plate; PCF: photonic crystal fiber; Pol.; Glan-Thompson polarizer; PBS: polarizing beam splitter; DM; dichroic mirror; OL: objective lens; CL: condenser lens; PZS: piezo scanning stage; SPF: short-pass filter to reject the pump light; BS2: beam splitter used to observe beam spots; VND; variable neutral density filter; and CCD: charge-coupled device used to confirm the overlap of the beams. (b) SP: spectrograph; FB: fiber bundle; and PC: personal computer.

mm convex lens to fill the entrance pupil of the objective on the microscope. The white pulsed-light beam is split into the probe and reference beams by a broadband polarizing beam splitter (PBS) (PBS252, THORLABS). The splitting intensity ratio is adjusted by the polarizer. The polarizer is also important to stabilize the polarization plane. The polarization plane of the SC light fixed with a PCF may be randomly rotating by a small amount of angle for pulse after pulse, even when the PCF is the polarization-maintaining type. The fluctuation of the polarization plane results in a fluctuation in the intensity splitting ratio due to the splitting-ratio dependency on polarization. Not only PBSs but also other beam splitters have this polarization dependency. Therefore, the stabilization of the polarization plane is essential to cancel out the intensity noise of the probe pulse. The reference beam is delayed for about a half cycle of repetition through an additional optical path, and then spatially overlapped and aligned collinearly

with the probe beam on the PBS. The wavelength components of larger than ~780 nm in the probe and reference lights are rejected by a slightly inclined from normal incidence 800-nm cut-off interference dichroic mirror (DM) (FES0800, THORLABS).

The 37% of reflected pump beam intensity at BS1 is sent to a delay stage to adjust the arrival time on the sample and ensures that it overlaps temporally only with the probe beam. The beam is chopped at a frequency of 4.48 kHz with a mechanical chopper (Model 3501, New Focus). The beam is guided to the 1.5× inverted Galilean telescope with a $f = -200$-mm concave lens and $f = 300$-mm convex lens to fill the entrance pupil of the objective on the microscope. The pump, probe, and reference beams are overlapped on the DM and are aligned to be collinear. The beams are input to a 40×, NA = 0.85 objective and tightly focused on the sample. The sample is placed on a computer-controlled piezo-scanning stage (MAX311D/M, THORLABS). The light reflected from the sample is collected with the objective and reflected by a pellicle beam splitter (BS2) with 92% T and 8% R to a CCD camera to confirm the spatial overlap of the beams. The lights transmitted through the sample are collimated by a condenser lens (NA = 1.4). The wavelength components that are longer than 780 nm in the probe and reference lights with 800-nm pump light are removed by the inclined 800-nm cut-off interference short-pass filter (FES0800, THORLABS).

The probe beam and reference beam are coupled with an optical fiber (LG-455-020, ACTON) by a convex lens (f = 50 mm) and sent to a 300-mm focal-length spectrograph (SpectraPro-300i, ACTON) equipped with a 1200 g/mm grating (Fig. 3(b)). The specified resolution power is 0.1 nm, and the dispersion is 2.7 nm/mm. The entrance slit width is set to 250 μm and the spectrum is imaged onto the facet of a 16 × 128 quartz fiber bundle array in the spectrograph. The core and clad diameters are 100 and 110 μm, respectively, and the entrance size is 1.8 × 16.5 mm. The spectrum is divided into 128 wavelengths, and each of the 16 fibers of the same wavelength component are bundled. A wavelength component is input into the present balanced detector. The synchronous signal for the sign flipping is accessed from the laser oscillator. The output from the balanced detector is input into a digital signal-processing lock-in amplifier (Model 7210, SIGNAL RECOVERY). The reference signal is generated by the chopper controller.

V. EXPERIMENT

A. Noise cancelling performance without resonator

The objective and condenser lenses on the microscope were removed and no sample was set. The 800-nm pump beam was blocked. A variable neutral density (ND) filter was inserted before the 50 mm convex lens for coupling with the optical fiber to adjust the optical input power. The spectra of the white probe light and the white reference light at the microscope were measured with a spectrometer (USB4000, Ocean Optics). The 643.07 nm component of the white light was coupled to the APD. The optical input power was measured at the output of the bundled optical fiber of 16 fibers from the spectrograph, which is coupled to the APD. The value of δ term was set to 0, and the noises were measured with the lock-in amplifier at a lock-in frequency of 4.48 kHz and the time constant of 1 s. The noises were evaluated as root-mean-square (RMS) values of 140 times measurements. The CN was evaluated by applying the 150 V reverse voltage-bias on the APD without optical input. First, to evaluate the optically balanced case, the value of B term was set to 0 and then chopped probe or reference light was input. The polarizer was adjusted so that the lights' outputs were equal. The noise of the probe light was evaluated by blocking the reference light and inputting the non-chopped probe light. The noise in balanced detection was evaluated by inputting both the probe and reference lights. Second, the optical powers of the probe and reference lights were displaced by adjusting the polarizer. The noises of the probe light and that in the balanced detection were measured as mentioned above. Third, the B term was applied so that the outputs of the chopped probe and reference lights were equal in maintaining that optical unbalance. The noises of the probe light and that in the balanced detection were evaluated.

B. Effect of resonator on a preamplifier

The optical setup was the same as in the case without the resonator. First, the optical delay of the reference light was set as half the cycle of the repetition, and the phase of the synchronous signal was set as 0 ($\Delta T = T/2$ and $\delta = 0$). The powers of the probe and reference lights were balanced by the polarizer, as mentioned above, and then the noise cancellation was evaluated. Second, the optical delay was set as a quarter cycle and the phase was adjusted as a quarter of π ($\Delta T = T/4$ and $\delta = \pi/4$). Then, the noise cancellation was evaluated. Third, the optical powers were unbalanced and the noise cancellation was measured. Fourth, the value of δ term was adjusted so that the outputs of the chopped probe and reference lights were balanced, and then the noise cancellation was evaluated.

C. Raman loss imaging of polystyrene beads

The Raman loss images of the PS beads were captured through the balanced detectors with or without the resonator. The observation wavelength was set to 643.07 nm, which corresponds to the 3050 cm^{-1} Raman shifts and the Raman band of the aromatic CH stretching mode of the PS. The sample was prepared as 4-μm PS beads on a glass slide. A dispersion of PS beads (Invitrogen) was dropped onto a glass slide and left to dry, and then covered by a 0.17-mm-thick cover-glass. In the imaging, the pump light was chopped at 4.48 kHz. For both circuits, the powers of the probe and reference lights were balanced, with the values of ΔT and δ set as $T/2$ and 0, respectively. The piezo stage and lock-in amplifiers are computer-controlled (LabVIEW 8.5 software), and the signals are observed point-by-point with the scanning of the sample.

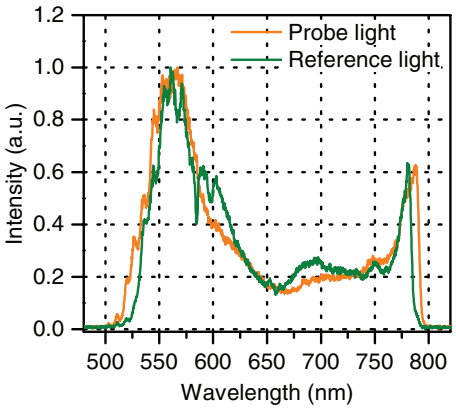

FIG. 4. Spectra of the white probe light and the white reference light at the microscope.

VI. RESULTS AND DISCUSSION

A. Noise cancelling performance without resonator

The spectra of the white probe and reference lights through DM at the microscope are mentioned in Fig. 4, and their spectra are different from each other due to the unbalanced parameters of the characteristics of the optics components. The outputs of the chopped probe and reference lights at various input powers of the probe light for the optically balanced case are shown in Table I. The optical unbalances are adjusted so that the output difference is smaller than 0.5%. Figure 5 shows the noise cancelling performance with the PA of the TIA. The red dotted line shows the actual measured CN without input light. The CN is 2.5×10^{-5} V/$\sqrt{\text{Hz}}$. This result clearly indicates the optical noise of the probe light (the orange plots in Fig. 5) is cancelled (the red plots) to the CN by this balanced detection. Figure 5(b) shows the normalized noise by the output of the chopped probe light. In this input power range, the noise cancelling performance is improved proportionally to the optical input power, since the performance is limited by the CN, which is independent on the input power. The maximum cancellation is 15 dB in this experimental condition (at the input power of 0.132 μW).

The optical unbalance is set as that the optical input powers of the probe and reference lights are set as 0.146 μW and 0.109 μW, and their outputs of the chopped lights are 1.10 V and 0.821 V, respectively. In this case, the probe noise (the light green triangle plots) is not completely cancelled and

TABLE I. Output signal intensities of the probe and reference lights with the TIA vs optical input power at the APD.

Power[a] (μW)	Pr[b] (V)	Ref[c] (V)
0.028	0.252	0.252
0.058	0.491	0.492
0.099	0.760	0.761
0.13	0.971	0.972

[a]Power: Optical input power of the probe light at the APD entrance.
[b]Pr: Output of only the chopped probe light through the balanced detector and the lock-in amplifier.
[c]Ref: Output of only the chopped reference light through the balanced detector and the lock-in amplifier.

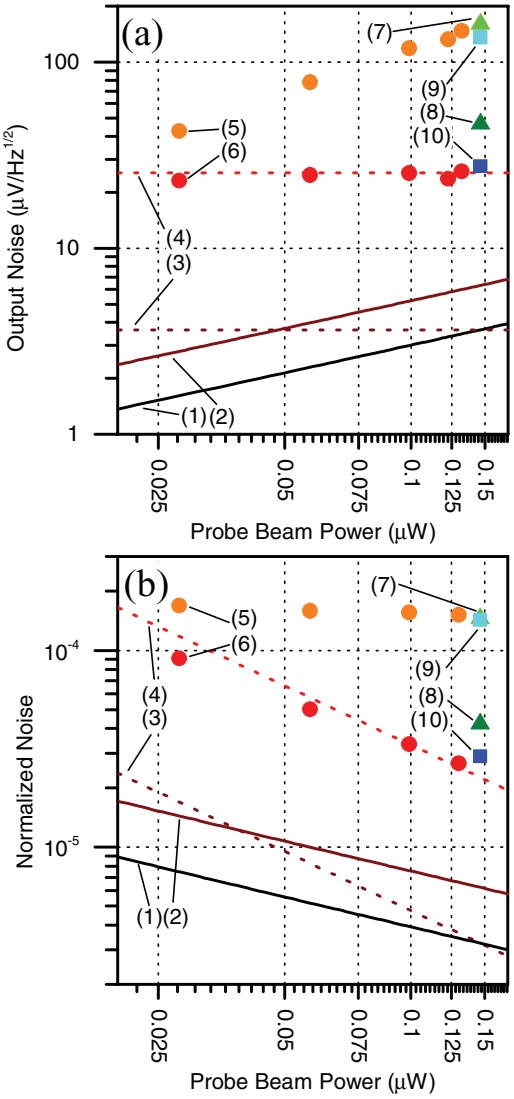

FIG. 5. Noise cancelling performance with the TIA vs optical input power of the probe light, and effect of the bias against the optical unbalance between the probe and reference lights. (1) and (2): calculated shot noise without and with the excess noise of the APD, respectively; (3) and (4): calculated and observed circuit noise; (5) and (6): noise on the probe light and that on the balanced detection in the optical balanced case; (7) and (8): those in the optical unbalanced case without the compensation; (9) and (10): those with the compensation by the bias. (a) Output RMS voltage and (b) normalized RMS voltage by the output of the chopped probe light.

5.3 dB residual noise remained toward the CN (the dark green triangle plots). This happens when white light is split into probe and reference lights; that is, when their powers are optically balanced at a particular wavelength, those in the different wavelengths are unbalanced due to the unbalance of the optics (Fig. 4). Therefore, although the optical noise at particular wavelengths can be completely cancelled out by adjusting the optical balance, the noises at different wavelengths cannot be cancelled out without some compensation. This effect requires the compensation on the detection side for the optical unbalanced parameters of optical components.

This unbalance is addressed by adjustment of the *B* term, so that the outputs of the probe and reference lights are 0.956 V and 0.953 V, respectively. With the addition of the *B* term, the noise of the probe light (light blue square plots) is

cancelled out (dark blue square plots) nearly to the CN (0.7 dB remained against the CN). This result demonstrates that the optical unbalance which is difficult to be eliminated using the optics can be addressed by the present balanced detector represented by the term B.

The lower-limit noise is determined not by the optical intensity noise or the SN, but by the CN of the circuit. The SN current with the APD is expressed as follows:

$$I_n^2 = 2q\left(I_L + I_{dg}\right) W M^2 F + 2q I_{ds} W. \quad (15)$$

Here, I_L, I_{dg}, I_{ds}, q, W, M, and F denote photocurrent without multiplication, dark current component multiplied, dark current component not multiplied, electron charge, bandwidth, multiplication ratio, and excess noise factor,[27] respectively. This SN is larger by the F value than that of the PIN photodiodes. In our experimental condition, M, I_d, F, and photo sensitivity at $M = 1$ are 105, 0.3 nA, 3.7, and 0.42 A/W, respectively. The black line in the Fig. 5 shows calculated output of the SN with the assumption of $F = 1$. The output gain in the calculation is the actual measured value. The brown solid and dotted lines are calculated SN and CN, respectively, with $F = 3.7$. This CN is calculated based on the thermal noise of the resistors and specifications of the active devices in the circuit. The value is 3.6×10^{-6} V/$\sqrt{}$Hz under the assumption that all components of the dark current shot noise are multiplied. Note that these calculated powers of the noise components are factored by 2 (and thus the output RMS voltage is $\sqrt{}2$ times) compared to one time measurement of the optical current, since a pair of the optical currents for the probe and reference lights are measured. The observed CN value is much larger than the calculated CN (17 dB larger). This large noise source is probably due to the exogenous noise, and thus we expect the performance is improved by reinforcing shields of the circuit and cables.

B. Effect of resonator on preamplifier

Table II shows the outputs of the chopped probe and reference lights from the circuit with and without the resonator, under the condition of optical balance, $\Delta T = T/2$ and $\delta = 0$. The optical unbalances are adjusted so that the output difference is less than 1%. The transimpedance gain with the RA is 507 kΩ at the resonant frequency and 2.9 times larger than that with the TIA (174 kΩ). The calculated and observed CN

TABLE II. Output signal intensities of the probe and reference lights with the RA vs optical input power at the APD.

Power[a] (μW)	Pr[b] (V)	Ref[c] (V)
0.020	0.491	0.491
0.040	0.978	0.976
0.062	1.47	1.46
0.088	1.96	1.96
0.102	2.18	2.20

[a]Power: Optical input power of the probe light at the APD entrance.
[b]Pr: Output of only the chopped probe light through the balanced detector and the lock-in amplifier.
[c]Ref: Output of only the chopped reference light through the balanced detector and the lock-in amplifier.

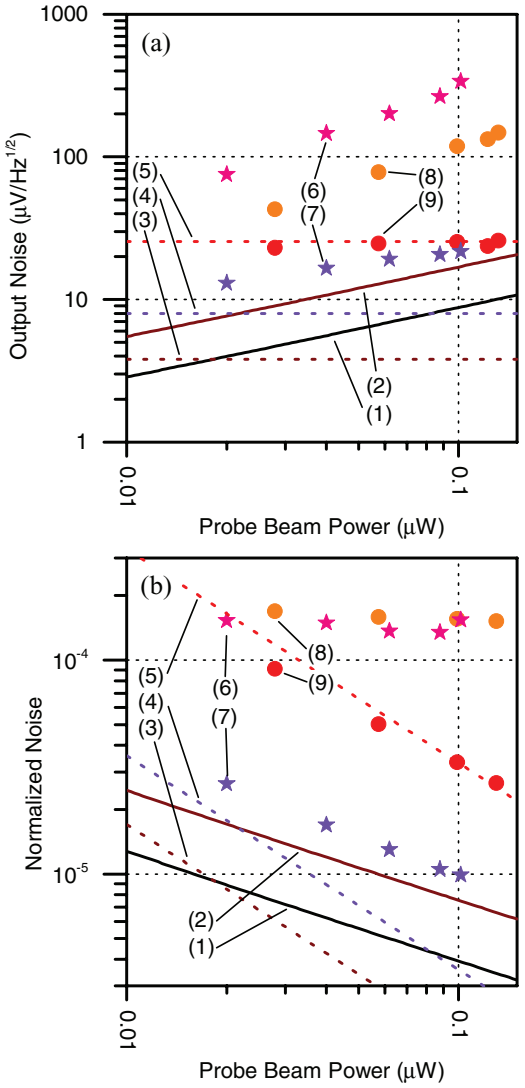

FIG. 6. Noise cancelling performance with the resonant pre-amplifier vs optical input power of the probe light. (1) and (2): calculated shot noise without and with the excess noise of the APD, respectively; (3) and (4): calculated and observed circuit noise; (5): the observed circuit noise with the TIA preamplifier for comparison; (6) and (7): noise on the probe light and that on the balanced detection; (8) and (9): those with the TIA. (a) Output RMS voltage and (b) normalized RMS voltage by the output of the chopped probe light.

with the RA are 3.8×10^{-6} V/$\sqrt{}$Hz (the brown dotted line in Fig. 6) and 8.0×10^{-6} V/$\sqrt{}$Hz (the purple dotted line), respectively, and the observed CN is closer to the calculated one (6.5 dB larger than calculated one) than that with the TIA. Despite the larger gain with the RA than with the TIA, the observed CN with the RA is smaller than that with the TIA (the red dotted line). This result explains rejection of the exogenous noise at other than the resonant frequency by the resonator.

The probe noise indicated by the pink star plots is cancelled to the purple star plots by the balanced detection, and this balanced detected noise is raised as the optical input is increased. This input-power dependence can be nearly fully explained by the calculated shot noise with the excess noise (the brown solid line). That is, the CN is reduced through rejection of the exogenous noise by the resonator, and, as a result, the

near SN (with the excess noise) limited noise-cancellation is attained. Just due to the larger gain of the PA with the RA, the probe light noise with the RA is larger than that with the TIA (the orange plots). To compare SNR between the circuits with and without the resonator, the normalized noise by the output of the probe light is shown in Fig. 6(b). Although the normalized probe-light noises with and without the resonator are nearly the same, the normalized balance-detected noise is significantly reduced with the resonator. This result demonstrates that the amplification of the signal and the rejection of the exogenous noise enhance the SNR by 11 dB at ~0.1 μW optical input, from the case without the resonator, and a 24 dB noise reduction is achieved at this optical intensity level.

One might assume that an increase in the Q value of the resonator still enhances the signal intensity and modifies the performance. The higher Q value, however, prolongs response time. Additionally, it results in a high susceptibility to the ambient conditions and instability of the signal phase, reducing robustness. The attachment of the resonator sacrifices the effect of the term B. In fact, when the optical balance is displaced, the B term cannot compensate for this unbalance. One method that enables the B term to compensate for the unbalance is providing a gain to the PA also for the DC component of the signal, for example, by inserting the parallel couple of a resister and a capacitor in series with the resonator. Another method is the half-wave rectification of the output from the PA.

However, another way to compensate for the optical unbalance is performed by adjusting the value of δ. As mentioned in Sec. II, a proper setting of ΔT as $T/4$ allows δ to compensate. In the optically balanced case, the outputs of the probe and reference lights at various optical input powers are shown in Table III, and the outputs differ in less than 1%. The gain is 383 kΩ and this value is 2.4 dB smaller than those in the case of $\Delta T = T/2$. This reduction is similar in value to 3 dB, as predicted by Eq. (13). Figure 7 shows the experimental results and theoretical calculations for the case of $\Delta T = T/4$. The black and brown solid lines indicate the calculated SN without and with excess noise. These values are reduced by 3 dB from those in Fig. 6 due to the gain reduction by 3 dB for optical current. The brown and purple dotted lines are the calculated and observed CN, respectively. They are independent of the ΔT and δ, and thus exactly the same as those in Fig. 6. The probe light noise (the orange pentagonal plots) is cancelled close to the calculated SN (the red pentagonal plots) also with this method, and 23 dB noise cancelling is attained with the 0.88 μW optical input power. The RMS voltage of the balance detected noise of this method is smaller than that of the $\Delta T = T/2$ case, due to the 3 dB smaller gain for the optical current containing the SN current. The normalized balance detected noise (red pentagonal plots in Fig. 7(b)) shows almost the same SNR as that of the $\Delta T = T/2$ case due to the near SN limited noise cancelling, in which the gain for the SN is also diminished by the same amount of the probe light from the $\Delta T = T/2$ case.

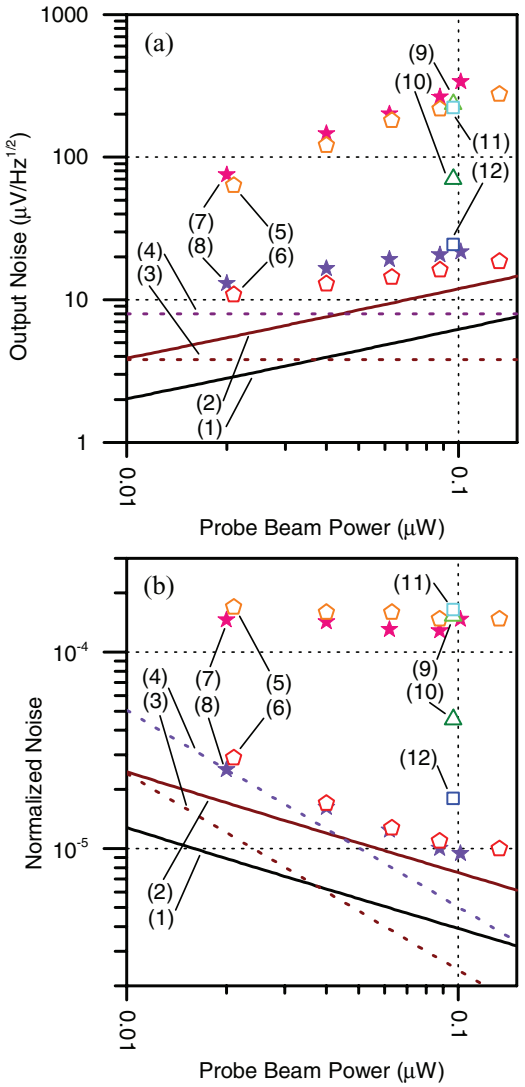

FIG. 7. Noise cancelling performance with the quarter cycle delay in the reference line vs optical input power of the probe light, and effect of the phase shift of the synchronous signal against the optical unbalance. (1) and (2): calculated shot noise without and with the excess noise of the APD, respectively; (3) and (4): calculated and observed circuit noise; (5) and (6): noise on the probe light and that on the balanced detection for the optical balanced case; (7) and (8): those with the half cycle delay in the reference line; (9) and (10): those in the optical unbalanced case without the compensation; (9) and (10): those with the compensation by the phase adjustment. (a) Output RMS voltage and (b) normalized RMS voltage by the output of the chopped probe light.

TABLE III. Output signal intensities of the probe and reference lights with the RA and the quarter cycle optical delay for the reference light vs optical input power at the APD.

Power[a] (μW)	Pr[b] (V)	Ref[c] (V)
0.021	0.376	0.374
0.040	0.760	0.761
0.063	1.12	1.13
0.088	1.48	1.47
0.133	1.86	1.86

[a]Power: Optical input power of the probe light at the APD entrance.
[b]Pr: Output of only the chopped probe light through the balanced detector and the lock-in amplifier.
[c]Ref: Output of only the chopped reference light through the balanced detector and the lock-in amplifier.

The optical unbalance is set in such a way that the optical input powers of the probe and reference lights are 0.097 μW and 0.072 μW respectively, and their outputs are 1.54 V and 1.20 V, respectively. In this case, the reduction of the probe noise by cancellation (the light green triangle plot) is 11 dB and the residual noise remains at a level of 15 dB toward the calculated SN (the dark green triangle plot). Then, the δ term is adjusted as the output voltages of the probe and reference lights are 1.35 V and 1.34 V, respectively. The noise cancellation is as large as 19 dB (the blue square plot) by this adjustment. This result clearly shows that the optical unbalance produced by the wavelength dependency of the optics can be corrected by the developed balanced detector by adjusting the δ term when the resonator is introduced to enhance the signal intensity.

Through this method, the compensation of the optical unbalance and the same amount of the enhancement of SNR by the resonator as in the case of $\Delta T = T/2$ are simultaneously attained with the adequate optical input power for the near SN limited performance, although the more optical input power is required by 3 dB than that for the $\Delta T = T/2$ case to achieve the SN limited performance.

C. Raman loss imaging of polystyrene beads

Figure 8 demonstrates the advantageous nature of the developed balanced detectors through stimulated Raman loss imaging captured on the 3050 cm^{-1} Raman band intensity. The upper panels (Figs. 8(a) and 8(b)) are observed through the TIA without the resonator and the lower panels (Figs. 8(c) and 8(d)) are observed through the resonant PA. The left (Figs. 8(a) and 8(c)) and the right (Figs. 8(b) and 8(d)) panels show the images without and with the reference light, respectively. The image and pixel sizes are 10 × 10 μm and 0.25 × 0.25 μm, respectively. The average power of the white probe beam and the power of the 800-nm pump beam are 4.3 and 78 mW, respectively, at the sample position, and the TC of the lock-in detection and dwelling times are 0.3 s and 0.6 s, respectively. The pseudo-color scales of all of the images are the same. Without the resonator, almost no modification of the image quality is observed (b). This is due to the low signal intensities of the probe and reference lights, and thus the Raman loss signal is at a comparable level with the CN through the reflection and the scattering by the sample. The main origin of the noise in image (a) is not the optical intensity fluctuation, which can be cancelled out, but the inextinguishable CN. However, the noise in image (c) is significantly reduced (d) with the resonator. The probe signal containing the Raman loss signal is sufficiently amplified over the CN by the resonator, and thus the principal noise in image (c) is not the CN, but the fluctuation in the probe light intensity. This optical fluctuation is successfully cancelled out by the reference signal, and the image is significantly modified (d).

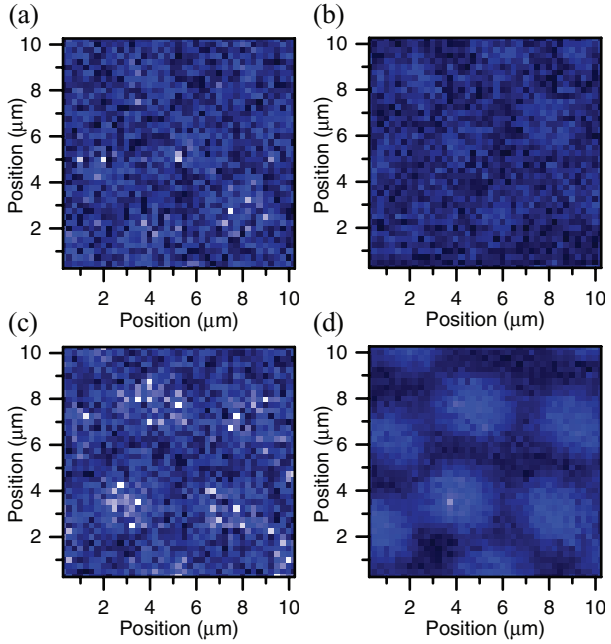

FIG. 8. Stimulated Raman loss images of the 4 μm polystyrene beads (10 × 10 μm area) through the balanced detectors. (a) The image captured through the transimpedance pre-amplifier without the resonator and without the reference light; (b) that with the reference light. (c) The image captured through the resonant pre-amplifier without reference light; (d) that with the reference light.

VII. CONCLUSION

We have developed a balanced detector with a single photodetector. The optical intensity unbalance between the probe and reference lights is electrically compensated by the present detector. Detection with a single photodetector enables the common optical path from a sample through a spectrograph to the detector. This is significantly advantageous in spectroscopy with a white probe light. The cancelling of noises non-correlated among wavelengths requires exactly the same spectral dispersions of the probe and reference lights. If their optical paths are different, two spectrometers are required in exactly the same condition, which significantly complicates the system and reduces its robustness. The common optical path is advantageous also for the application to imaging. The effects other than stimulations on the sample synchronous to the probe pulsed light can be also cancelled out, such as the reflection, the scattering, and the absorption through the sample.

The circuit can compensate for the optical unbalance to achieve complete noise cancellation of the white probe light, simultaneously, in whole wavelength region. The noise cancellation directly depends on the balance between the probe signal and the corresponding reference signal, and the highest improvement is achieved at the equal signal intensities between the two. Therefore, the maximum noise reduction in full wavelength range without the compensation requires equal optical splitting in the whole wavelength range, which is extremely difficult with the practically available optics. To cancel noise simultaneously in the broad wavelength range, this optical unbalance can be addressed by the developed balanced detectors, and the best improvement in SNR is attained simultaneously at any wavelength.

The sign flipping by the square wave renders it unnecessary to position the reference pulses rigorously at the center between the probe pulses. This produces easy adjustment of

the optical path length of the delay of the reference line. Additionally, it enables the application to low-repetition pulsed laser systems.

The signal amplification by the resonator on the photodetector effectively enhances SNR. However, the resonator attachment has two drawbacks. First, the phase differences among the signals and the synchronous signal of the pulse repetition sensitively affect the performance. Second, the term B cannot compensate for the optical unbalance due to the lack of the DC component in the output from the PA. However, the optical unbalance can be corrected by adjusting the values of ΔT and δ.

In this paper, the optical intensity balance between the probe and reference lights is addressed by manually adjusting a variable resistor or a variable capacitor. This scheme should be modified to an automated adjustment for practical applications to the multi-wavelength measurements, and this automation can be readily done with a feedback scheme similar to the auto-balance scheme based on the DC component from a LPF on the ML. The developed balanced detector develops a way to high speed multi-color, multi-modal imaging and sensing applications across various fields by retaining the relatively low-cost, facile handling of the PCF for the SC light generation, and by eliminating the significant noise problem.

ACKNOWLEDGMENTS

This study was financially supported by a joint research project at the Institute of Laser Engineering, Osaka University, under Contract No. B1-27.

[1]Y. Nagashima, T. Suzuki, S. Terada, S. Tsuji, and K. Misawa, J. Chem. Phys. **134**, 024525 (2011).
[2]F.-K. Lu, M. Ji, D. Fu, X. Ni, C. W. Freudiger, G. Holtom, and X. S. Xie, Mol. Phys. **110**, 1927–1932 (2012).
[3]W. Rock, M. Bonn, and S. H. Parekh, Opt. Express **21**, 15113–15120 (2013).
[4]J. M. Dudley, G. Genty, and S. Coen, Rev. Mod. Phys. **78**, 1135–1184 (2006).
[5]D. M. Owen, E. Auksorius, H. B. Manning, C. B. Talbot, P. A. A. de Beule, C. Dunsby, M. A. A. Neil, and P. M. W. French, Opt. Lett. **32**, 3408–3410 (2007).
[6]D. Wildanger, E. Rittweger, L. Kastrup, and S. W. Hell, Opt. Express **16**, 9614–9621 (2008).
[7]K. Isobe, W. Watanabe, S. Matsunaga, T. Higashi, K. Fukui, and K. Itoh, Jpn. J. Appl. Phys. **44**, L167 (2005).
[8]M. Okuno, H. Kano, P. Leproux, V. Couderc, J. P. R. Day, M. Bonn, and H. Hamaguchi, Angew. Chem., Int. Ed. **49**, 6773–6777 (2010).
[9]K. Bito, M. Okuno, H. Kano, P. Leproux, V. Couderc, and H. Hamaguchi, Chem. Phys. **419**, 156–162 (2013).
[10]H. T. Beier, G. D. Noojin, and B. A. Rockwell, Opt. Express **19**, 18885–18892 (2011).
[11]K. Seto, Y. Okuda, E. Tokunaga, and T. Kobayashi, Rev. Sci. Instrum. **84**, 083705–083709 (2013).
[12]E. R. Andresen, P. Berto, and H. Rigneault, Opt. Lett. **36**, 2387–2389 (2011).
[13]B. R. Bachler, M. E. Fermann, and J. P. Ogilvie, Opt. Express **20**, 835–844 (2012).
[14]U. Møller, S. T. Sørensen, C. Jakobsen, J. Johansen, P. M. Moselund, C. L. Thomsen, and O. Bang, Opt. Express **20**, 2851–2857 (2012).
[15]J. N. Ames, S. Ghosh, R. S. Windeler, A. L. Gaeta, and S. T. Cundiff, Appl. Phys. B **77**, 279–284 (2003).
[16]K. L. Corwin, N. R. Newbury, J. M. Dudley, S. Coen, S. A. Diddams, K. Weber, and R. S. Windeler, Phys. Rev. Lett. **90**, 113904 (2003).
[17]N. R. Newbury, B. R. Washburn, K. L. Corwin, and R. S. Windeler, Opt. Lett. **28**, 944–946 (2003).
[18]K. L. Corwin, N. R. Newbury, J. M. Dudley, S. Coen, S. A. Diddams, B. R. Washburn, K. Weber, and R. S. Windeler, Appl. Phys. B **77**, 269–277 (2003).
[19]D. R. Solli, B. Jalali, and C. Ropers, Phys. Rev. Lett. **105**, 233902 (2010).
[20]D. R. Solli, C. Ropers, and B. Jalali, Phys. Rev. Lett. **101**, 233902 (2008).
[21]N. Brauckmann, M. Kues, P. Groß, and C. Fallnich, Opt. Express **19**, 14763–14778 (2011).
[22]A. Gambetta, V. Kumar, G. Grancini, D. Polli, R. Ramponi, G. Cerullo, and M. Marangoni, Opt. Lett. **35**, 226–228 (2010).
[23]M. Celebrano, P. Kukura, A. Renn, and V. Sandoghdar, Nat. Photon. **5**, 95–98 (2011).
[24]See supplementary material at http://dx.doi.org/10.1063/1.4863879 for intensity noises at different wavelengths and circuit diagrams.
[25]P. C. D. Hobbs, Appl. Opt. **36**, 903–920 (1997).
[26]K. Nose, Y. Ozeki, T. Kishi, K. Sumimura, N. Nishizawa, K. Fukui, Y. Kanematsu, and K. Itoh, Opt. Express **20**, 13958–13965 (2012).
[27]R. J. McIntyre, IEEE Trans. Electron Devices **13**, 164–168 (1966).